



Published in final edited form as:

Neuroimage. 2012 February 15; 59(4): 3075–3084. doi:10.1016/j.neuroimage.2011.11.030.

TE-Dependent Spatial and Spectral Specificity of Functional Connectivity

Changwei W. Wu^{1,2}, Hong Gu¹, Qihong Zou³, Hanbing Lu¹, Elliot A. Stein¹, and Yihong Yang¹

¹Neuroimaging Research Branch, National Institute on Drug Abuse, National Institutes of Health, Baltimore, MD, United States

²Institute of Biomedical Engineering, National Central University, Taoyuan, Taiwan

³MRI Research Center and Beijing City Key Lab for Medical Physics and Engineering, Peking University, Beijing, 100871, China

Abstract

Previous studies suggest that spontaneous fluctuations in the resting-state fMRI (RS-fMRI) signal may reflect fluctuations in transverse relaxation time (T_2^*) rather than spin density (S_0). However, such S_0 and T_2^* features have not been well characterized. In this study, spatial and spectral characteristics of functional connectivity on sensorimotor, default-mode, dorsal attention, and primary visual systems were examined using a multiple gradient-echo sequence at 3T. In the spatial domain, we found broad, local correlations at short echo times (TE = 14 ms) due to dominant S_0 contribution, whereas long-range connections mediated by T_2^* became explicit at TEs longer than 22 ms. In the frequency domain, compared with the flat spectrum of S_0 , spectral power of the T_2^* -weighted signal elevated significantly with increasing TE, particularly in the frequency ranges of 0.008-0.023 Hz and 0.037-0.043 Hz. Using the S_0 spectrum as a reference, we propose two indices to measure spectral signal change (SSC) and spectral contrast-to-noise ratio (SCNR), respectively, for quantifying the RS-fMRI signal. These indices demonstrated TE dependency of connectivity-related fluctuation strength, resembling functional contrasts in activation-based fMRI. These findings further confirm that large-scale functional circuit connectivity based on BOLD contrast may be constrained within specific frequency ranges in every brain network, and the spectral features of S_0 and T_2^* could be valuable for interpreting and quantifying RS-fMRI data.

Keywords

fMRI; spontaneous fluctuations; functional connectivity; echo time; frequency

Please send correspondences to: Yihong Yang, Ph.D. Neuroimaging Research Branch, National Institute on Drug Abuse, NIH 251 Bayview Blvd, Suite 200 Baltimore, MD 21224 YihongYang@intra.nida.nih.gov Tel: (443)740-2648.

Publisher's Disclaimer: This is a PDF file of an unedited manuscript that has been accepted for publication. As a service to our customers we are providing this early version of the manuscript. The manuscript will undergo copyediting, typesetting, and review of the resulting proof before it is published in its final citable form. Please note that during the production process errors may be discovered which could affect the content, and all legal disclaimers that apply to the journal pertain.

Presented at ISMRM 19th scientific meeting, Montreal, Canada, 2011

INTRODUCTION

Since the first resting-state functional MRI (RS-fMRI) study was reported (Biswal et al., 1995), there has been growing interest in utilizing the technique to investigate system-level “functional connectivity” circuits within the brain (Buckner et al., 2008; Raichle et al., 2001; Zhang and Raichle, 2010). The temporal correlation of low-frequency spontaneous fluctuations between brain regions based on blood oxygenation level dependent (BOLD) contrast (Ogawa et al., 1992) is thought to reflect transient neuronal synchrony during unconstrained, on-going cognitive processes (Biswal et al., 1995; Fox et al., 2007; Vincent et al., 2007). Due to its ability to map brain connectivity without the requirement of specific task-performance, this functional connectivity method has shed light on neurobiological investigations, on the neuropathology of several prominent disorders including Alzheimer's disease (Li et al., 2002; Zhou et al., 2010), multiple sclerosis (Lowe et al., 2002; Roosendaal et al., 2010), depression (Anand et al., 2005), schizophrenia (Bluhm et al., 2007), autism (Cherkassky et al., 2006), and substance addiction (Gu et al., 2010; Hong et al., 2009). Despite the proliferation of functional connectivity studies, the neurobiological mechanisms underlying endogenous spontaneous activity in RS-fMRI fluctuations is still to be fully determined. It is generally hypothesized that the source of spontaneous BOLD fluctuations is primarily from neuronal activity. Further, these fluctuations seem to be related to specific frequency ranges within underlying electrophysiological signals (Laufs et al., 2003; Lu et al., 2007; Shmuel and Leopold, 2008), suggesting that the RS-fMRI signal originates mainly from synchronized neural activity (Varela et al., 2001).

Beyond the source of spontaneous neural activity, the RS-fMRI signal may contain various non-neural sources such as thermal noise, head motion, respiratory and cardiac pulsations, and scanner instabilities, which could impact functional connectivity (Bianciardi et al., 2009; Birn et al., 2006; Shmueli et al., 2007). Bianciardi et al. (2009) estimated that only half of the RS-fMRI signal in gray matter can be explained by spontaneous activity at the ROI level at 7 T, indicating the necessity of removing non-neural sources during data processing. To this end, a number of processing methods have been developed to remove or minimize potential noise arising from respiratory and cardiac pulsations (Beall and Lowe, 2007; Birn et al., 2008; Glover et al., 2000).

Spontaneous fluctuations can reflect both spin density (S_0) fluctuations and transverse relaxation time (T_2^*) fluctuations. Peltier and Noll (2002) reported that the functional connectivity signal stems from perturbations of magnetic susceptibility (or T_2^* modulations); however, the origin of S_0 fluctuations in the RS-fMRI signal remain largely unknown. Previous studies using multi-echo strategies attempted to develop theoretical models to decompose the BOLD signal into multiple TE-dependent source/noise components, including physiological fluctuations (Krüger and Glover, 2001; Wu and Li, 2005). Krüger and Glover (2001) assumed that the sources of S_0 and T_2^* are uncorrelated, while Wu and Li (2005) demonstrated that the magnitude of S_0 fluctuations decay monoexponentially with echo time (TE), but T_2^* contributions reached a maximum value at TE around 50 ms at 3T. These models indicated that both S_0 and T_2^* significantly contribute to fMRI signals and imply that understanding their contribution to spontaneous fMRI fluctuations could help to interpret the connectivity phenomenon. However, knowledge about S_0 and T_2^* weightings in functional connectivity is still very limited. Hence, a systematic characterization of resting-state BOLD signal using a multi-TE strategy is necessary and would provide insights into the physiological basis of functional connectivity.

Spatial specificity is the most prominent feature in functional connectivity studies. Using the multi-echo method, Peltier and Noll (2002) demonstrated no significant functional connectivity patterns at TE of 7.7 ms. Yan et al. (2009) showed that the magnitude of signal

driftreached maximum at $TE = T_2^*$ in gray matter, attenuated monotonically with increasing TE in white matter, and increased monotonically in cerebrospinal fluid (CSF). This evidence indicated the diversity of TE dependencies of spontaneous fluctuations across brain tissue types, suggesting that such variability of TE dependency could also exist among brain networks. On the other hand, the TE-dependent S_0 and T_2^* contributions (Wu and Li, 2005) suggest that the connectivity-related spectral power varies with TE and thus can be used as a candidate for noise removal or quantification of the RS-fMRI signal. In the current study, our working hypothesis was that both spatial and spectral specificity of functional connectivity exhibit TE dependencies, providing diverse contributions from S and T_2^* at multiple TEs in brain networks. We used a multi-echo, gradient-echo sequence at 3T to investigate the spatial patterns and frequency distributions with TEs ranging from 7.7 ms to 60 ms. TE-dependent spatial disparities and frequency bands were demonstrated within motor, attention, default-mode, and visual cortical networks.

MATERIALS AND METHODS

Participants

Ten healthy subjects (4 males, age: 24 ± 3 years) were recruited for participation in this study. All subjects were screened with a questionnaire to ensure that they had no history of neurological illness, psychiatric disorders, or drug abuse. Current drug use and pregnancy were assessed with urine tests. Informed consent was obtained from all participants prior to the experiments in accordance with the protocol approved by the Institutional Review Board of the National Institute on Drug Abuse, Intramural Research Program.

MRI acquisition

MRI experiments were performed on an Allegra 3T scanner (Siemens, Erlangen, Germany) using a head volume coil. Head motion was minimized using individually custom-made foam padding. Thirty-five axial slices (220×220 mm² field of view, 64×64 in-plane matrix size, and 4 mm slice thickness without gap) aligned along the anterior commissure – posterior commissure plane were prescribed in an interleaved fashion. Prior to the functional scans, all subjects were instructed to rest with their eyes closed, not to think of anything in particular, and not to fall asleep. Four functional datasets were acquired while the subjects were under such a “resting state”. A custom-made four-echo gradient-refocused echo planar imaging (EPI) sequence was used to collect the first two datasets with partial k-space (6/8) acquisition, repetition time (TR) of 3 s, flip angle of 87° and 200 measurements for each dataset. The TEs were 7.7, 22, 37, 52 ms for the first set, and 14, 30, 45, 60 ms for the second set. The other two functional datasets, acquired using a typical spin-echo EPI sequence, were not associated with the working hypothesis in this study, and are not further discussed. After the functional scans, a total of 19 non-slice-selective inversion recovery EPI images were acquired with multiple inversion times (TIs: 30 80 130 180 230 330 430 530 630 730 830 1030 1230 1530 1830 2230 2730 3230 3830 ms) for structural segmentation. For spatial normalization and localization, a set of high-resolution T_1 -weighted anatomical images (3D-MPRAGE with $256 \times 192 \times 160$ matrix size; $1 \times 1 \times 1$ mm³ in-plane resolution; TI = 1000 ms; TR/TE = 2500/4.38 ms; flip angle = 8°) was acquired on each subject.

Pre-processing

Functional data were processed using the Analysis of Functional Neuroimaging (AFNI) software package (Cox, 1996). Motion correction was performed by volume registering each 3D dataset to a base volume (both translation and rotation were less than 0.7 mm for all subjects). Linear detrending was applied to eliminate first-order (linear) drift induced by system instability but preserved baseline information. Subsequently, using signal intensity of each four-echo dataset, S_0 and T_2^* time courses were least-square fitted for all voxels via an

exponential model: $S = S_0 \cdot \exp\left(-\frac{TE}{T_2^*}\right)$. Each functional dataset was low-pass-filtered at the cutoff frequency of 0.1 Hz using Chebyshev type II filters in MATLAB (MathWorks, Inc., CA). The edges of the cutoff frequency were constrained within 6 dB decay in the passband, while at least 30 dB attenuation was guaranteed in the stopband. All images were then normalized to Talairach space and resampled to an isotropic resolution ($3 \times 3 \times 3 \text{ mm}^3$) with linear interpolation. Spatial smoothing was applied using a Gaussian isotropic kernel (full width at half maximum of 6 mm) to minimize the effect of individual variances and to enhance the signal-to-noise ratio. Considering the potential influence of physiological noise, estimations of cardiac and respiratory information were performed using physiological estimation by temporal independent component analysis (PESTICA) on each dataset (Beall and Lowe, 2007). Specifically, twelve independent components were identified by temporal ICA, and a single component maximally correlated with a predefined cardiac-relevant map was considered as the major source of cardiac response. The time course retrieved from this component was then regarded as a cardiac estimator. The same procedure was carried out to generate a respiratory estimator. Linear regression analyses of these cardiac and respiratory estimators were then used to remove potential physiological influence. In addition, a T_1 map was fit for each subject using the 19 multiple TI inversion recovery EPI images, allowing segmentation into gray matter, white matter, and cerebrospinal fluid (CSF) maps using a custom linear decomposition algorithm in MATLAB (probability = 0.9). The white matter and CSF maps were used as masks for retrieving signal time courses for subsequent regression analysis.

Statistical analysis

Spherical seeds (6 mm in diameter), chosen from the right side of the brain, were prescribed for four cortical networks based on previous literature (Van Dijk et al., 2010; Wu et al., 2008): 1) primary motor cortex [36, -28, 54] of the sensorimotor network (Motor); 2) posterior cingulate cortex [4, -53, 26] of the default-mode network (Default); 3) frontal eye field [40, -4, 48] of the dorsal attention network (Attention); and 4) primary visual cortex [4, -81, 8] of the visual network (Visual). Seed-based correlation was employed to examine the temporal correlation between brain areas using a linear regression analysis, including ten nuisance covariates (six motion parameters, the physiological estimators of respiratory and cardiac noise, and the global estimators retrieved from the segmented white matter and CSF masks). Then the correlation maps were transformed using Fisher's Z-transformation

$\left(z = \frac{1}{2} \log\left(\frac{1+cc}{1-cc}\right)\right)$, where CC represents correlation coefficients) to approach a normal distribution. Additionally, the amplitude of low-frequency fluctuation (ALFF) was used as a second index to estimate the regional intensity of spontaneous fluctuations from 0-0.1 Hz (Yang et al., 2007) and normalized to 0 Hz. Second-level group analyses were performed in AFNI using mixed-effects ANOVA for both z-transformed CC and ALFF. Corrections for multiple comparisons were performed by estimating the family-wise error based on spatial correlation and cluster size, yielding an overall false positive $p < 0.05$ (uncorrected $p < 0.003$, with a minimum cluster volume of 1323 mm^3), as determined by Monte Carlo simulations. To minimize potential bias in comparing results from the multi-echo datasets, regions of interest (ROIs) for each cortical network were defined from the S_0 - and T_2^* -based connectivity maps. While calculating the mean CC or ALFF within the ROIs, the seed points were excluded to prevent overestimation of the functional indices. Estimated T_2^* values in the cortical networks were retrieved from the same ROIs for further evaluations of the optimal TE.

RESULTS

Fig. 1a shows the functional connectivity maps for four brain networks using each of the eight echoes (7.7 to 60 ms), corresponding to the S_0 and T_2^* connectivity maps. The functional connectivity maps with ultra-short echoes (7.7 and 14 ms) demonstrate broad local spatial extent and less long-range connections, resembling the results derived from S_0 . Long-distance connections became evident and consistent in connectivity maps at TE of 22 ms and longer in all networks. Some distant connections shrank slightly in size (e.g. Motor and Visual networks) at relatively long TEs (52 and 60 ms). Imposing T_2^* -based ROIs, connectivity indices (CC and ALFF) as a function of TE are illustrated in Fig. 1b and 1c, respectively. Second-order, least-squares polynomial fits demonstrate the trends within each network ($r^2 > 0.64$ and 0.92 for CC and ALFF, respectively). Both indices reached maxima at TE between 30 and 45 ms, contingent on the network observed. Estimated T_2^* and optimal TEs retrieved from CC and ALFF are listed in Table 1. In spite of moderate variations across brain networks, the optimal TEs calculated by CC and ALFF were slightly shorter than T_2^* values.

To examine the spatial variability within each network, S_0 and T_2^* connectivity ROIs from Fig. 1a are displayed separated into S_0 -only (green), T_2^* -only (red) and S_0 - T_2^* overlap (orange) masks in Fig. 2. Connectivity strengths (i.e., CC) in the masks are plotted in Fig. 3. Coefficient values within the overlap mask generally maintain a sustained and maximal level in each network, whereas those within the T_2^* -only masks display similar convex patterns as in Fig. 1b. Nonetheless, CCs within the S_0 -only mask decreased with increasing TE, indicating less functional connections at long TE.

To account for the disparities of temporal signal-to-noise ratio (from 82 to 308) in the multi-echo dataset, power spectra were all normalized to the power of its direct current (DC, 0 Hz), corresponding to the mean signal in the temporal domain, and then averaged across subjects. Using a stationary fast-Fourier transform algorithm, we transformed the time courses of the multi-echo dataset and the S_0 dataset (equal to TE=0) for spectral comparison. Fig. 4 illustrates the spectral variations within the three masks of each network as a function of TE. Generally, the S_0 spectra across networks were almost flat across all frequencies, except at less than 0.01 Hz, and the spectral power was elevated as TE increased. The enhancement of low-frequency power was prominent, especially in the range between 0.01 and 0.05 Hz, within the T_2^* - and overlap masks, whereas increased power was less noticeable in S_0 -only masks. Only the first dataset with four echoes are shown here for spectral comparison because they were acquired simultaneously in the same session; similar characteristics were seen in the frequency domain dataset.

The flat power spectra from the S_0 mask and the TE-dependent spectral enhancement from the T_2^* and overlap masks in Fig. 4 demonstrate that S_0 fluctuations are relatively TE irrelevant and less specific in their frequency response. Lack of spectral and spatial specificity in functional connectivity made S_0 a candidate as a baseline reference for other TE-dependent signals. Hence, using S_0 as a reference, the fine spectral resolution (0.0017 Hz) allowed us to seek the most significant bands sensitive to T_2^* weighting, which may be responsible for long-distance connectivity and might be related to hemodynamic oscillations from electrophysiological rhythms. Therefore, we conducted a two-sample t-test with unequal variance comparing the power spectra from each TE and the power spectrum from S_0 , respectively. Results are shown in Fig. 5, in which the statistical significance is color-coded in gray ($p < 0.01$) and black ($p < 0.005$) across subjects. It was noted that spectra at low TEs were not significantly different from those in S_0 ($p > 0.05$), whereas the significant enhancements were observed in several specific frequency bands at longer TEs. The frequency bands showing significant differences were [0.008-0.015, 0.035-0.050] Hz in

motor system, [0.008-0.022, 0.035-0.043] Hz in default-mode network, [0.008-0.020] Hz in dorsal attention network, and [0.008-0.023, 0.043-0.052, 0.063-0.068, 0.082-0.093] Hz in visual system.

Another perspective of using S_0 as a reference is to quantify the contrast for functional connectivity, which has been unavailable in RS-fMRI, as opposed to activation-based fMRI. Since the noise-like feature of S_0 exhibits in the frequency domain, we defined spectral

signal change as $SSC = \frac{\sum_{0.01}^{0.1} P_{TE}}{\sum_{0.01}^{0.1} P_{S_0}} - 1$, and spectral contrast-to-noise ratio as $SCNR = \frac{\bar{P}_{TE} - \bar{P}_{S_0}}{\sqrt{\sigma_{TE}^2 + \sigma_{S_0}^2}}$, where \bar{P}_{TE} is the average spectral power at each TE over 0.01 – 0.1 Hz, \bar{P}_{S_0} is the average spectral power of S_0 over the same frequency range, σ_{TE} and σ_{S_0} are spectral standard deviation at each TE and of S_0 over 0.01 – 0.1 Hz, respectively. Fig. 6 demonstrates these two indices versus echo time. An approximate linear relationship between SSC and TE was found across all four brain networks (Fig. 6a, $r^2 > 0.94$). SCNR showed a convex pattern similar to what was found in CC and ALFF, and the optimal TE values estimated by SCNR approximated the T_2^* values (Table 1). Data for SCNR were fit with second-order polynomials (Fig. 6b, $r^2 > 0.97$).

As a control analysis for neural activity, a seed in CSF (center at the right lateral ventricle [6, 2, 20]) was applied and identical analyses conducted as described above. Fig. 7a shows connectivity maps across TEs using the same statistical power, where the spatial patterns within ventricles were found to be unrelated to or independent of TE. A CSF mask was generated by retrieving common connected areas across TEs and then used as a mask to calculate CC and spectral power. In contrast to cortical networks, the mean CC within ventricles (Fig. 7b) was relatively flat without significant differences between echo times. Power spectra in CSF (Fig. 7c) also lacked of significant differences among the TEs ($p > 0.3$).

DISCUSSION

In this study, the TE-dependent spatial specificity and spectral distribution of resting state functional connectivity were examined using a multi-echo strategy at 3T. In the spatial domain, we found that the regionally confined connectivity patterns at short TEs (7.7 and 14 ms) had strong S_0 contribution, suggesting that RS-fMRI with an ultra-short TE may not be feasible for mapping systems level, long-range functional connections. In contrast, the flat S_0 spectrum in the frequency domain indicated relative TE independence and less frequency response specificity. Thus, due to its lack of spectral and spatial specificity, the estimated S_0 signal was chosen as a reference for its non-BOLD noise contribution. Using this strategy and comparing the S_0 spectra to the spectra from multi-echo signals, we localized the most prominent T_2^* -weighted frequency ranges in four cortical-based intrinsic networks. These results not only confirm the observation that functional connectivity is based on spontaneous T_2^* fluctuations, but also disclosed specific connectivity-associated frequency ranges. In addition, two quantification indices, spectral signal change (SSC) and spectral contrast-to-noise ratio (SCNR) are proposed as contrast measures for resting-state functional connectivity, resembling signal change and CNR observations from activation-based fMRI. Even though both indices were estimated voxel-wise, the TE-dependency of SCNR resembles that of CC and ALFF, and the signal maxima of SCNR was closer to T_2^* than CC and ALFF (Table 1). Using S_0 as a non-BOLD reference, it is suggested that SCNR can serve as a potential index to quantify functional connectivity.

Spatial specificity

It is generally assumed that spontaneous fluctuations in neural activity is reflected in the T_2^* -weighted RS-fMRI signal. In our study, the TE dependency in connectivity levels (ALFF and CC, Fig. 1b and 1c, respectively) resembled previous CNR models of task-based fMRI (Hyde et al., 2001; Menon et al., 1993). Robust long-range connectivity in T_2^* -based connectivity maps (Fig. 1a) also demonstrated that intrinsic network connectivity patterns result from fluctuations based on BOLD contrast. In contrast, remote connections appeared absent at short TEs (7.7 and 14 ms), similar to the S_0 -based connectivity patterns (Fig. 1), indicating dominant S_0 contributions in these short-TE signals. The flat S_0 spectra of functional networks (Fig. 4) and overall flat spectra of CSF regions (Fig. 7) suggest that the S_0 perturbations do not likely contribute to spontaneous BOLD activity. This speculation was supported by water phantom scans, resulting in similar broad, locally correlated spatial regions as seen in S_0 maps of Fig. 1a (data not shown). Such neural-activity independent S_0 fluctuations may originate from several possible sources: baseline blood inflow effects, vasomotor perturbations, steady-state free precession (SSFP) effect of CSF, instrument noise, and B_0 fluctuations. However, vasomotor variability not only changes S_0 but may also changes blood oxygenation levels, and thus changes T_2^* as well. In our experiments, SSFP effects of CSF had little consequence on the RS-fMRI signal since a relatively long TR (3 s) was used, compared to the 1.8-2.2 s T_2 of human CSF (Zhao et al., 2000). Baseline inflow effects, caused by velocity variations of blood flow, may contribute to S_0 fluctuations while the baseline oxygenation remains at the same level (Gao et al., 1996). Instrument noise and B_0 fluctuations caused by residual physiological noise and/or head motion may also contribute to both S_0 and T_2^* fluctuations. To control for neuronal activity independent noise, it would thus seem reasonable to adopt S_0 fluctuations as a reference when quantifying RS-fMRI contrast (Fig.6).

Another interesting finding in the present study is the unmatched spatial specificity between S_0 and T_2^* maps and their regional coherence. As mentioned above, broad local connectivity dominated the S_0 maps, which may represent undesirable non-neuronal contributions, while the T_2^* -dependent connectivity may represent neuronal activity. However, overlapped brain regions (Fig. 2, orange color) in the four networks demonstrate maintained correlation coefficients at a certain level (0.3~0.4 on average) across all TEs (Fig. 3). This suggests that the sustained correlation coefficients might be due to similar spatial autocorrelation caused by preprocessing (smoothing and normalization), independent of the signal sources.

On the other hand, given the same imaging parameters and spatial smoothing processes, the connectivity-based point spread function should center on the seed points with a fixed size. However, as demonstrated in Fig. 2, overlapping regions were not necessarily centered on seed points and the spatial extent varied across networks. Similar to the hypothesis underlying regional homogeneity (ReHo), functional connectivity should occur in clusters, exhibiting intrinsic local boundaries between connected brain areas (Zang et al., 2004). Previously, Massimini measured a localized electrical response instead of long-distance propagation in human premotor cortex using transcranial magnetic stimulation during sleep (Massimini et al., 2005). Lu et al. (2007) also observed that long-distance somatosensory connections in rats were reduced with increasing anesthesia levels, while short-distance connections remained relatively unaffected. The maintenance of local connectivity regardless of BOLD contrast or anesthesia could be due to such physiological variables as the inflow effect, sharing the same vascular source or cell-swelling (Le Bihan, 2007), but remains to be investigated further.

An alternative conjecture for the absence of distant connections at short TEs is the differential vascular weighting of the BOLD signal across TEs. Previous studies showed that the contribution to the BOLD signal from the extravascular (EV) compartment increases

with long TEs, while the intravascular (IV) contribution dominates at short TEs (Hulvershorn et al., 2005; Silvennoinen et al., 2003). Hence, the reduced remote connections and elevated local connections at short TEs may be caused by signal fluctuations dominated from the IV compartment. The signal fluctuations in the microvascular EV compartment may reflect primarily endogenous neural synchrony, while the oscillations in the IV fluctuations may be more modulated by the neighboring circulatory system independent of neural activity, resulting in broad local functional connections but sparse distant ones. Unfortunately, the relative IV/EV contributions in the current study cannot be determined from the existing dataset. Further studies that include diffusion-weighted sequences would enable the evaluation of IV/EV weightings in signal fluctuations.

Spectral specificity

The power density of the RS-fMRI signal (with appropriate T_2^* weighting) possessed $1/f$ characteristics. This phenomenon is not unique to the fMRI signal (Fox et al., 2007; Zarahn et al., 1997) but rather is a common feature observed in electrophysiological studies (Leopold et al., 2003; Linkenkaer-Hansen et al., 2001), implying a common biological feature of neural oscillations (Buzsáki and Draguhn, 2004). Previous studies have shown the spectral behavior in resting-state fMRI signal over a relatively wide frequency range (0-1.25 Hz), demonstrating the effects of both slow fluctuations and physiological noise on a variety of networks (Cordes et al., 2001; Salvador et al., 2008; Wu et al., 2008; Zuo et al., 2010). However, due to the lack of spectral resolution, uncertainty of the frequency range specific to spontaneous fluctuations makes it difficult to relate fMRI fluctuations with underlying electrophysiology signals. In the current work, we determined the most significant frequency ranges that were enhanced by T_2^* weightings with a finer spectral resolution (0.0017 Hz) in each intrinsic network (Fig. 5). Both the T_2^* mask and overlay mask, with similar T_2^* weighting along echo times, generated similar spectral results over the observed frequency range. It is worth mentioning that the advantage of high spectral resolution can be further improved by prolonged acquisition time using a multi-echo comparison in each session.

Though slight variability occurred in each network, common T_2^* -specific frequency ranges were located between 0.008-0.023 Hz and 0.037-0.043 Hz in the “resting” human brain. In motor, default, and visual networks, a relatively small peak was also found around 0.082-0.092 Hz. Interestingly, similar frequency bands have been reported for functional connectivity networks. Chang and Glover (2010) found that fMRI fluctuations in the default-mode network had positive coherence at 0.015 Hz using a time-frequency coherence analysis. Using multichannel near-infrared spectroscopy, Sasai et al. (2011) demonstrated that resting oxyhemoglobin fluctuations peaked at 0.009-0.02 and 0.06-0.08 Hz. These studies support our findings of spectral specificity in hemodynamic fluctuations using fMRI.

Several studies using simultaneous electrophysiology and fMRI measurements across multiple species indicated direct association between resting neural and hemodynamic responses, especially in the high-gamma (>30 Hz) and low frequency (2-15 Hz) bands between functionally related areas (Mantini et al., 2007; Schölvinck et al., 2010; Shmuel and Leopold, 2008). These electrophysiological bands may be the main source of the most sensitive bands within the fMRI fluctuations observed in our study. However, even considering the intrinsic hemodynamic filter, the frequency mismatch between the two modalities appears to exhibit strong nonlinearity when propagating from neural oscillations to blood oxygenation variations. Thus, the neurobiological mechanism for this coupling remains unanswered, and further investigation using multi-modal measurements is warranted.

Signal change and CNR

Seed-based correlation coefficients and goodness of fit from independent component analysis have been long used as indices of functional connectivity strength. Other local indices have also been proposed, such as ALFF, fractional ALFF, and ReHo (Yang et al., 2007; Zang et al., 2004; Zou et al., 2008), and have been applied to clinical studies comparing neuropathological patients to healthy controls. However, the stationary analysis of such current indices might confound the outcome by involving connectivity-irrelevant factors without any compensating references (except regressors). Therefore, in this study, the proposed metrics, i.e. SSC and SCNR, were all normalized to S_0 , the major difference from previous indices.

Given that S_0 provides purely connectivity-irrelevant information and that BOLD contrast is at least part of the source of the observed spontaneous activity, both SSC and SCNR were able to quantify functional connectivity in large-scale cortical networks. With an identical definition of signal change as used in traditional fMRI analysis, SSC showed an approximately linear relationship with TE, similar to that found in correlation coefficients and activation-based fMRI studies (Menon et al., 1993; Peltier and Noll, 2002; Yang et al., 1998), indicating a linear elevation of spectral power (i.e., the standard deviation of low-frequency fluctuations in the time domain) with echo times, suggesting that the connectivity-induced functional contrast is based on the BOLD mechanism (similar trends are also present in the spectral power of Fig. 4 and p-values of Fig. 5).

However, this phenomenon may not reflect the spontaneous fluctuations throughout brain regions because it was estimated voxel-wise without interactions with other voxels. Furthermore, the linear association between spectral power and TE is somewhat contrary to previous reports on baseline fMRI fluctuations using phantom or human brain, where the amplitude of baseline fluctuations could be a convex function of TE (Krüger and Glover, 2001; Wu and Li, 2005). This is due to the disparity of normalizing to the DC power. The drop-down at long TE caused the SNR reduction regardless of T_2^* weightings, supported by the relative/absolute drift magnitude (Yan et al., 2009) and is also seen in the ALFF results (Fig. 1c). On the other hand, the definition of SCNR in this study was amended from Hyde's modified CNR model (Eq. [3] of Hyde et al., 2001), transforming it into a comparison between average power of TE-dependent data and S_0 within the low frequency band.

A saturated SCNR was found at TE approximating T_2^* values in the four intrinsic networks (Fig. 6), indicating its high sensitivity to fluctuations induced by T_2^* . These indices can also be applied to other functional imaging sequences such as spin echo, perfusion-based or diffusion-weighted fMRI sequences to estimate detailed biophysical variability. Nevertheless, it should be noted that both indices are based on fluctuation amplitude rather than connectivity strength. Further refinements, such as time-frequency coherence analysis or S_0 - T_2^* conjunction noise modeling, may be needed prior to quantitative evaluations of functional connectivity.

Finally, the proposed metrics using S_0 as a reference may not be practical since they required multi-echo acquisitions. An alternative strategy is to adopt an additional session of RS-fMRI with an ultra-short TE. At TE of 7.7 ms, both spatial patterns and frequency spectra were not significantly different from those of S_0 , suggesting they could be used as an approximation of non-BOLD noise. Since instrument and thermal noise is white and time-invariant across sessions, the S_0 variations between sessions were statistically insignificant ($p > 0.4$). However, acquiring the short-TE dataset in a different session requires separate preprocessing steps including motion correction, spatial registration, and physiological noise regression. Although these steps should be exercised with caution, it is still a practical strategy to estimate SNR metrics using S_0 or ultra-short-TE signal as the reference.

CONCLUSIONS

TE-dependent spatial and spectral specificity were evaluated in motor, default-mode, dorsal attention, and visual networks. The lack of long-range connectivity and the absence of low-frequency power at short TEs indicated the dominance of S_0 contribution, which revealed the spatial correlations of distributed noise sources unrelated to spontaneous neuronal fluctuations. Taking S_0 spectrum as a reference, we observed T_2^* -mediated frequency ranges specific to each brain network and assessed the efficacy of functional connectivity by introducing two spectral indices for quantifying RS-fMRI signal. These findings, based on a multi-echo strategy, provide further insights into the T_2^* dependency of spontaneous fluctuations in RS-fMRI that may be valuable when interpreting and quantifying functional connectivity data.

Acknowledgments

This work was supported by the Intramural Research Program of the National Institute on Drug Abuse (NIDA), National Institutes of Health (NIH) and National Science Council of Taiwan (NSC98-2917-I-564-158).

REFERENCES

- Anand A, Li Y, Wang Y, Wu J, Gao S, Bukhari L, Mathews VP, Kalnin A, Lowe MJ. Activity and connectivity of brain mood regulating circuit in depression: a functional magnetic resonance study. *Biol Psychiatry*. 2005; 57:1079–1088. [PubMed: 15866546]
- Beall EB, Lowe MJ. Isolating physiologic noise sources with independently determined spatial measures. *Neuroimage*. 2007; 37:1286–1300. [PubMed: 17689982]
- Bianciardi M, Fukunaga M, van Gelderen P, Horovitz SG, de Zwart JA, Shmueli K, Duyn JH. Sources of functional magnetic resonance imaging signal fluctuations in the human brain at rest: a 7 T study. *Magn Reson Imaging*. 2009; 27:1019–1029. [PubMed: 19375260]
- Birn RM, Diamond JB, Smith MA, Bandettini PA. Separating respiratory-variation-related fluctuations from neuronal-activity-related fluctuations in fMRI. *Neuroimage*. 2006; 31:1536–1548. [PubMed: 16632379]
- Birn RM, Smith MA, Jones TB, Bandettini PA. The respiration response function: the temporal dynamics of fMRI signal fluctuations related to changes in respiration. *Neuroimage*. 2008; 40:644–654. [PubMed: 18234517]
- Biswal B, Yetkin FZ, Haughton VM, Hyde JS. Functional connectivity in the motor cortex of resting human brain using echo-planar MRI. *Magn Reson Med*. 1995; 34:537–541. [PubMed: 8524021]
- Bluhm RL, Miller J, Lanius RA, Osuch EA, Boksman K, Neufeld RW, Théberge J, Schaefer B, Williamson P. Spontaneous low-frequency fluctuations in the BOLD signal in schizophrenic patients: anomalies in the default network. *Schizophr Bull*. 2007; 33:1004–1012. [PubMed: 17556752]
- Buckner RL, Andrews-Hanna JR, Schacter DL. The brain's default network: anatomy, function, and relevance to disease. *Ann N Y Acad Sci*. 2008; 1124:1–38. [PubMed: 18400922]
- Buzsáki G, Draguhn A. Neuronal oscillations in cortical networks. *Science*. 2004; 304:1926–1929. [PubMed: 15218136]
- Chang C, Glover GH. Time-frequency dynamics of resting-state brain connectivity measured with fMRI. *Neuroimage*. 2010; 50:81–98. [PubMed: 20006716]
- Cherkassky VL, Kana RK, Keller TA, Just MA. Functional connectivity in a baseline resting-state network in autism. *Neuroreport*. 2006; 17:1687–1690. [PubMed: 17047454]
- Cox RW. AFNI: software for analysis and visualization of functional magnetic resonance neuroimages. *Comput Biomed Res*. 1996; 29:162–173. [PubMed: 8812068]
- Cordes D, Haughton VM, Arfanakis K, Carew JD, Turski PA, Moritz CH, Quigley MA, Meyerand ME. Frequencies contributing to functional connectivity in the cerebral cortex in “resting-state” data. *Am J Neuroradiol*. 2001; 22(7):1326–33. [PubMed: 11498421]

- Fox MD, Snyder AZ, Vincent JL, Raichle ME. Intrinsic fluctuations within cortical systems account for intertrial variability in human behavior. *Neuron*. 2007; 56:171–184. [PubMed: 17920023]
- Gao JH, Miller I, Lai S, Xiong J, Fox PT. Quantitative assessment of blood inflow effects in functional MRI signals. *Magn Reson Med*. 1996; 36:314–319. [PubMed: 8843386]
- Glover GH, Li TQ, Ress D. Image-based method for retrospective correction of physiological motion effects in fMRI: RETROICOR. *Magn Reson Med*. 2000; 44:162–167. [PubMed: 10893535]
- Gu H, Salmeron BJ, Ross TJ, Geng X, Zhan W, Stein EA, Yang Y. Mesocorticolimbic circuits are impaired in chronic cocaine users as demonstrated by resting-state functional connectivity. *Neuroimage*. 2010; 53:593–601. [PubMed: 20603217]
- Hong LE, Gu H, Yang Y, Ross TJ, Salmeron BJ, Buchholz B, Thaker GK, Stein EA. Association of nicotine addiction and nicotine's actions with separate cingulate cortex functional circuits. *Arch Gen Psychiatry*. 2009; 66:431–441. [PubMed: 19349313]
- Hulvershorn J, Bloy L, Gualtieri EE, Redmann CP, Leigh JS, Elliott MA. Temporal resolving power of spin echo and gradient echo fMRI at 3T with apparent diffusion coefficient compartmentalization. *Hum Brain Mapp*. 2005; 25:247–258. [PubMed: 15849715]
- Hyde JS, Biswal BB, Jesmanowicz A. High-resolution fMRI using multislice partial k-space GR-EPI with cubic voxels. *Magn Reson Med*. 2001; 46:114–125. [PubMed: 11443717]
- Krüger G, Glover GH. Physiological noise in oxygenation-sensitive magnetic resonance imaging. *Magn Reson Med*. 2001; 46:631–637. [PubMed: 11590638]
- Laufs H, Krakow K, Sterzer P, Eger E, Beyerle A, Salek-Haddadi A, Kleinschmidt A. Electroencephalographic signatures of attentional and cognitive default modes in spontaneous brain activity fluctuations at rest. *Proc Natl Acad Sci U S A*. 2003; 100:11053–11058. [PubMed: 12958209]
- Le Bihan D. The 'wet mind': water and functional neuroimaging. *Phys Med Biol*. 2007; 52:R57–90. [PubMed: 17374909]
- Leopold DA, Murayama Y, Logothetis NK. Very slow activity fluctuations in monkey visual cortex: implications for functional brain imaging. *Cereb Cortex*. 2003; 13:422–433. [PubMed: 12631571]
- Li SJ, Li Z, Wu G, Zhang MJ, Franczak M, Antuono PG. Alzheimer Disease: evaluation of a functional MR imaging index as a marker. *Radiology*. 2002; 225:253–259. [PubMed: 12355013]
- Linkenkaer-Hansen K, Nikouline VV, Palva JM, Ilmoniemi RJ. Long-range temporal correlations and scaling behavior in human brain oscillations. *J Neurosci*. 2001; 21:1370–1377. [PubMed: 11160408]
- Lowe MJ, Phillips MD, Lurito JT, Mattson D, Dzemidzic M, Mathews VP. Multiple sclerosis: low-frequency temporal blood oxygen level-dependent fluctuations indicate reduced functional connectivity initial results. *Radiology*. 2002; 224:184–192. [PubMed: 12091681]
- Lu H, Zuo Y, Gu H, Waltz JA, Zhan W, Scholl CA, Rea W, Yang Y, Stein EA. Synchronized delta oscillations correlate with the resting-state functional MRI signal. *Proc Natl Acad Sci U S A*. 2007; 104:18265–18269. [PubMed: 17991778]
- Mantini D, Perrucci MG, Del Gratta C, Romani GL, Corbetta M. Electrophysiological signatures of resting state networks in the human brain. *Proc Natl Acad Sci U S A*. 2007; 104:13170–13175. [PubMed: 17670949]
- Massimini M, Ferrarelli F, Huber R, Esser SK, Singh H, Tononi G. Breakdown of cortical effective connectivity during sleep. *Science*. 2005; 309:2228–2232. [PubMed: 16195466]
- Menon RS, Ogawa S, Tank DW, Urbil K. Tesla gradient recalled echo characteristics of photic stimulation-induced signal changes in the human primary visual cortex. *Magn Reson Med*. 1993; 30:380–386. [PubMed: 8412612]
- Ogawa S, Tank DW, Menon R, Ellermann JM, Kim SG, Merkle H, Ugurbil K. Intrinsic signal changes accompanying sensory stimulation: functional brain mapping with magnetic resonance imaging. *Proc Natl Acad Sci U S A*. 1992; 89:5951–5955. [PubMed: 1631079]
- Peltier SJ, Noll DC. T(2)(*) dependence of low frequency functional connectivity. *Neuroimage*. 2002; 16:985–992. [PubMed: 12202086]
- Raichle ME, MacLeod AM, Snyder AZ, Powers WJ, Gusnard DA, Shulman GL. A default mode of brain function. *Proc Natl Acad Sci U S A*. 2001; 98:676–682. [PubMed: 11209064]

- Roosendaal SD, Hulst HE, Vrenken H, Feenstra HE, Castelijns JA, Pouwels PJ, Barkhof F, Geurts JJ. Structural and functional hippocampal changes in multiple sclerosis patients with intact memory function. *Radiology*. 2010; 255:595–604. [PubMed: 20413769]
- Salvador R, Martínez A, Pomarol-Clotet E, Gomar J, Vila F, Sarró S, Capdevila A, Bullmore E. A simple view of the brain through a frequency-specific functional connectivity measure. *Neuroimage*. 2008; 39:279–289. [PubMed: 17919927]
- Sasai S, Homae F, Watanabe H, Taga G. Frequency-specific functional connectivity in the brain during resting state revealed by NIRS. *Neuroimage*. 2011; 56:252–257. [PubMed: 21211570]
- Schölvinck ML, Maier A, Ye FQ, Duyn JH, Leopold DA. Neural basis of global resting-state fMRI activity. *Proc Natl Acad Sci U S A*. 2010; 107:10238–10243. [PubMed: 20439733]
- Shmuel A, Leopold DA. Neuronal correlates of spontaneous fluctuations in fMRI signals in monkey visual cortex: Implications for functional connectivity at rest. *Hum Brain Mapp*. 2008; 29:751–761. [PubMed: 18465799]
- Shmueli K, van Gelderen P, de Zwart JA, Horovitz SG, Fukunaga M, Jansma JM, Duyn JH. Low-frequency fluctuations in the cardiac rate as a source of variance in the resting-state fMRI BOLD signal. *Neuroimage*. 2007; 38:306–320. [PubMed: 17869543]
- Silvennoinen MJ, Clingman CS, Golay X, Kauppinen RA, van Zijl PC. Comparison of the dependence of blood R2 and R2* on oxygen saturation at 1.5 and 4.7 Tesla. *Magn Reson Med*. 2003; 49:47–60. [PubMed: 12509819]
- Van Dijk KR, Hedden T, Venkataraman A, Evans KC, Lazar SW, Buckner RL. Intrinsic functional connectivity as a tool for human connectomics: theory, properties, and optimization. *J Neurophysiol*. 2010; 103:297–321. [PubMed: 19889849]
- Varela F, Lachaux JP, Rodriguez E, Martinerie J. The brainweb: phase synchronization and large-scale integration. *Nat Rev Neurosci*. 2001; 2:229–239. [PubMed: 11283746]
- Vincent JL, Patel GH, Fox MD, Snyder AZ, Baker JT, Van Essen DC, Zempel JM, Snyder LH, Corbetta M, Raichle ME. Intrinsic functional architecture in the anaesthetized monkey brain. *Nature*. 2007; 447:83–86. [PubMed: 17476267]
- Wu CW, Gu H, Lu H, Stein EA, Chen JH, Yang Y. Frequency specificity of functional connectivity in brain networks. *Neuroimage*. 2008; 42:1047–1055. [PubMed: 18632288]
- Wu G, Li SJ. Theoretical noise model for oxygenation-sensitive magnetic resonance imaging. *Magn Reson Med*. 2005; 53:1046–1054. [PubMed: 15844094]
- Yan L, Zhuo Y, Ye Y, Xie SX, An J, Aguirre GK, Wang J. Physiological origin of low-frequency drift in blood oxygen level dependent (BOLD) functional magnetic resonance imaging (fMRI). *Magn Reson Med*. 2009; 61:819–827. [PubMed: 19189286]
- Yang H, Long XY, Yang Y, Yan H, Zhu CZ, Zhou XP, Zang YF, Gong QY. Amplitude of low frequency fluctuation within visual areas revealed by resting-state functional MRI. *Neuroimage*. 2007; 36:144–152. [PubMed: 17434757]
- Yang Y, Glover GH, van Gelderen P, Patel AC, Mattay VS, Frank JA, Duyn JH. A comparison of fast MR scan techniques for cerebral activation studies at 1.5 tesla. *Magn Reson Med*. 1998; 39:61–67. [PubMed: 9438438]
- Zang Y, Jiang T, Lu Y, He Y, Tian L. Regional homogeneity approach to fMRI data analysis. *Neuroimage*. 2004; 22:394–400. [PubMed: 15110032]
- Zarahn E, Aguirre GK, D'Esposito M. Empirical analyses of BOLD fMRI statistics. I. Spatially unsmoothed data collected under null-hypothesis conditions. *Neuroimage*. 1997; 5:179–197. [PubMed: 9345548]
- Zhang D, Raichle ME. Disease and the brain's dark energy. *Nat Rev Neurol*. 2010; 6:15–28. [PubMed: 20057496]
- Zhao X, Bodurka J, Jesmanowicz A, Li SJ. B(0)-fluctuation-induced temporal variation in EPI image series due to the disturbance of steady-state free precession. *Magn Reson Med*. 2000; 44:758–765. [PubMed: 11064411]
- Zhou J, Greicius MD, Gennatas ED, Growdon ME, Jang JY, Rabinovici GD, Kramer JH, Weiner M, Miller BL, Seeley WW. Divergent network connectivity changes in behavioural variant frontotemporal dementia and Alzheimer's disease. *Brain*. 2010; 133:1352–1367. [PubMed: 20410145]

- Zou QH, Zhu CZ, Yang Y, Zuo XN, Long XY, Cao QJ, Wang YF, Zang YF. An improved approach to detection of amplitude of low-frequency fluctuation (ALFF) for resting-state fMRI: fractional ALFF. *J Neurosci Methods*. 2008; 172:137–141. [PubMed: 18501969]
- Zuo XN, Di Martino A, Kelly C, Shehzad ZE, Gee DG, Klein DF, Castellanos FX, Biswal BB, Milham MP. The oscillating brain: complex and reliable. *Neuroimage*. 2010; 49:1432–1445. [PubMed: 19782143]

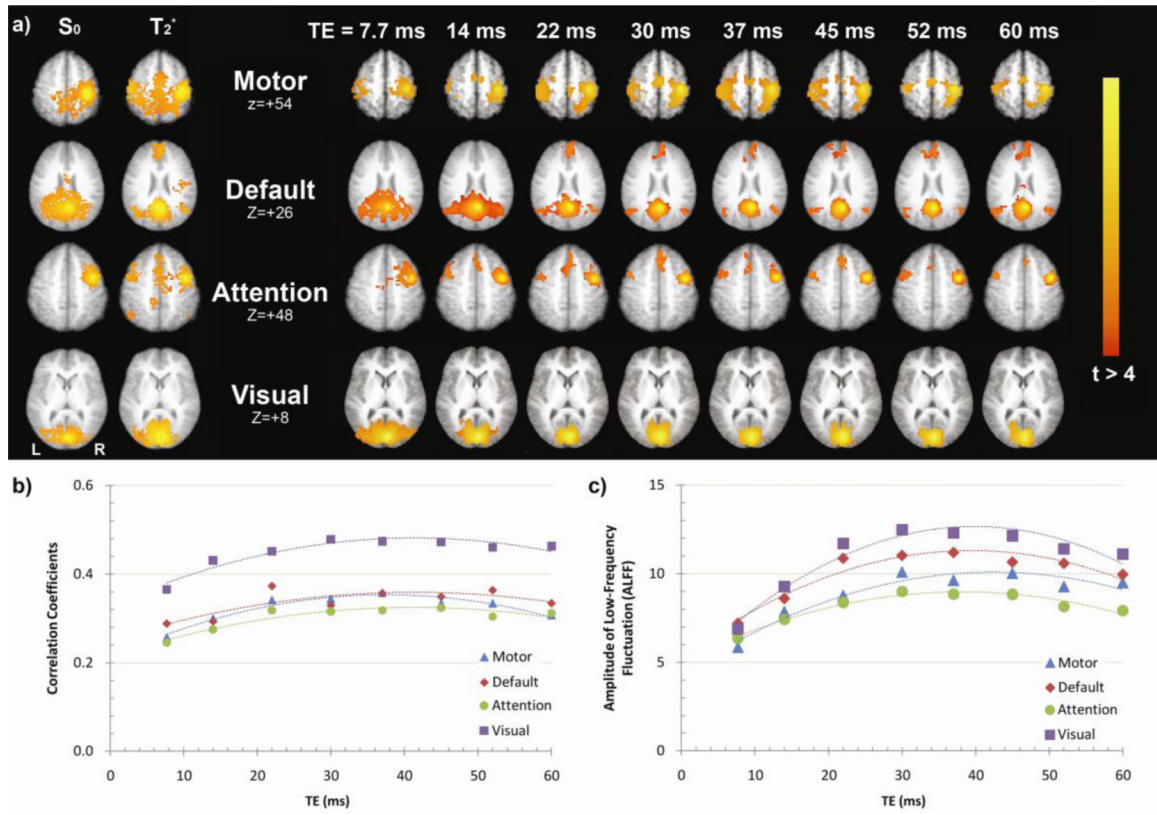


Figure 1.

a) Multi-TE based functional connectivity maps of intrinsic cerebral networks, overlaid on high-resolution anatomical images. S₀ and T₂^{*} maps were generated from the first of two multi-echo datasets. The location of each slice is based on where each brain network's seed point is located. Average connectivity indices of b) CC and c) ALFF are plotted as a function of TE. Second-order polynomial fittings ($R^2 > 0.64$ and 0.92 for CC and ALFF, respectively) are overlaid and used for estimating optimal TE in each network.

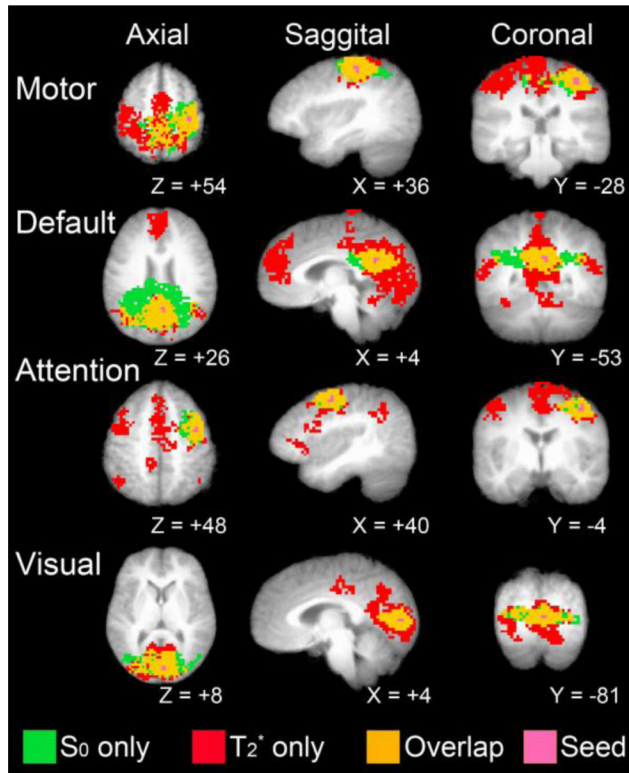


Figure 2. Connectivity masks of S and T₂^{*} retrieved from Fig. 1, shown in three dimensions. S₀-only (green) masks spread broadly whereas long-range connections are seen in T₂^{*}-only (red) masks. Overlap (orange) regions locally surround the location of seed points. Seed sources (pink) were excluded from all the masks.

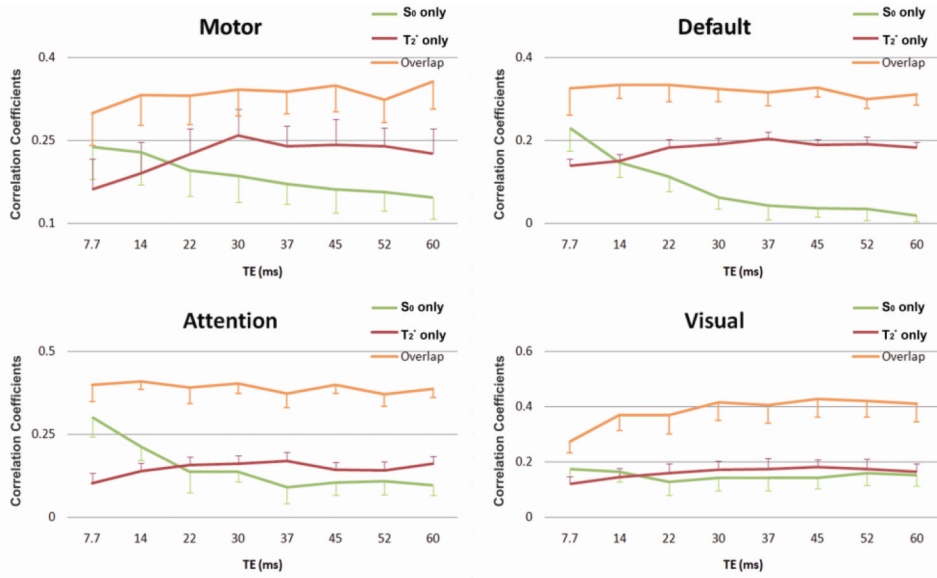


Figure 3. Average correlation coefficients across echo times within S₀-only (green), T₂^{*}-only (red) and overlap (orange) masks, respectively, as described in Fig. 2. Note that correlations from the T₂^{*} mask (red) reach a plateau whereas correlations from the S₀ mask (green) gradually decrease with increasing TE. Error bars (± SEM) represent the variability across subjects.

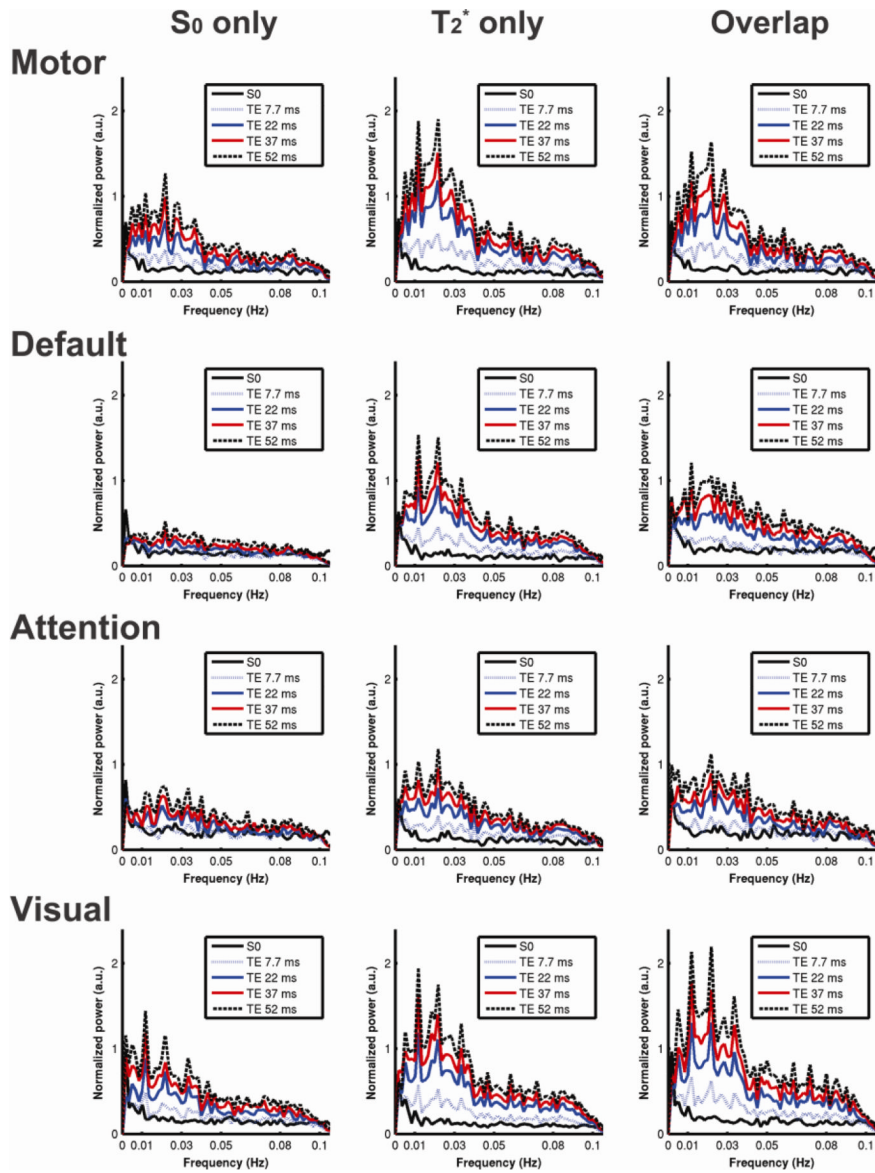


Figure 4. Average power spectra proportional to TE across subjects. The spectral features differ from mask regions in four intrinsic networks. Only spectra from the first data set with TEs of 7.7, 22, 37, 52 ms and S_0 are shown for simplicity, which are normalized to their DC values.

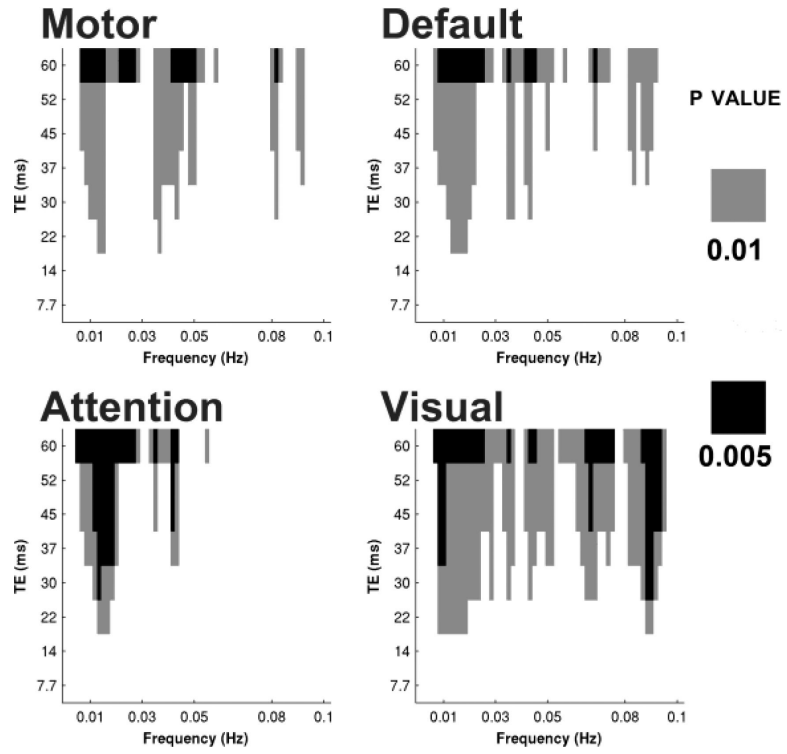


Figure 5. Significance level indicating the enhanced frequency bands along with echo times based on the T_2^* -only mask in the four brain networks. Significance is defined as p-value (one-tail, two-sample with spectral points excluding DC) across subjects and color-coded as gray for $p < 0.01$ and black for $p < 0.005$.

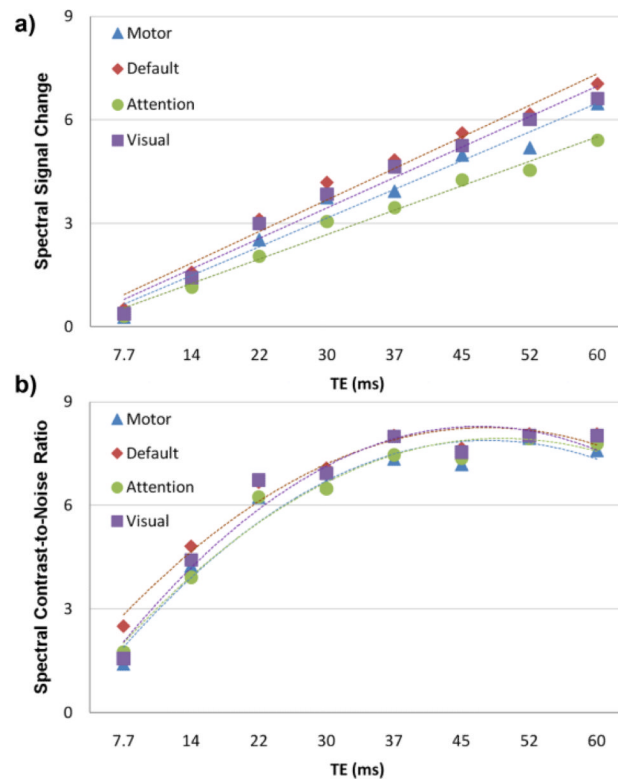


Figure 6. Average connectivity-contrast indices, a) spectral signal change and b) spectral contrast-to-noise ratio, as a function of TE in four intrinsic networks. Linear trend lines ($r^2 > 0.94$) are overlaid on (a) while second-order polynomial fittings ($r^2 > 0.97$) are overlaid on (b) for each network and adopted for estimating optimal TE.

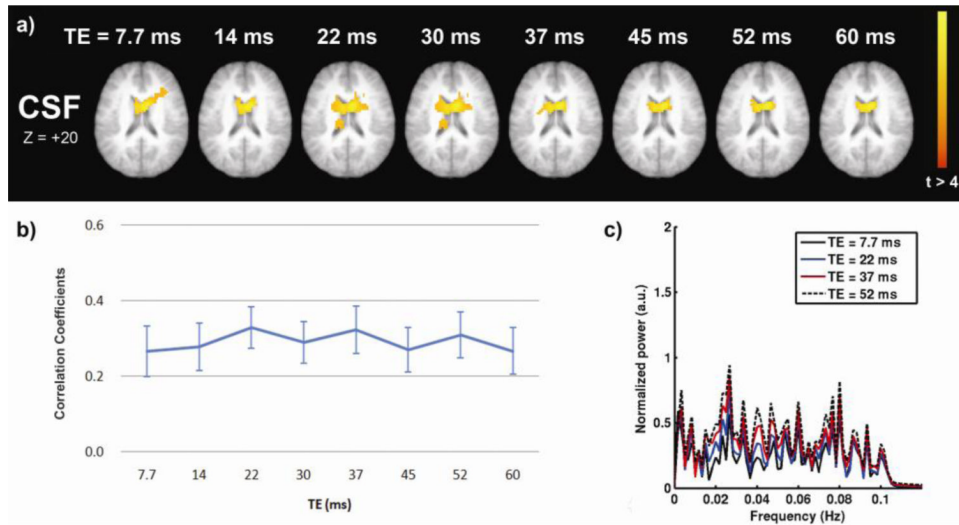


Figure 7.

a) Functional connectivity maps based on CSF seeding with eight echo times, overlaid on a high-resolution anatomical image. b) Correlation coefficients along echo times, extracted from an averaged connectivity mask. Error bars (\pm STD) represent between-subject variability. c) Spectral distributions with four echoes from the first dataset.

Table 1

Optimal TEs estimated from correlation coefficients (CC), amplitude of low-frequency fluctuation (ALFF), and spectral contrast-to-noise ratio (SCNR) by fitting the gradient-echo signal with eight echo times and the T_2^* fit for each network.

	Estimated T_2^*	Optimal TE (CC)	Optimal TE (ALFF)	Optimal TE (SCNR)
Motor	45.5	38.0	42.7	45.9
Default	46.1	39.2	38.7	43.4
Attention	45.5	38.6	38.1	46.9
Visual	44.4	41.1	39.8	44.8
Average	45.4	39.2	39.8	45.3